



# Effects of unequal blockage ratio and obstacle spacing on wave speed and overpressure during flame propagation in stoichiometric $H_2/O_2$

C. Brunoro Ahumada<sup>1</sup> · Q. Wang<sup>1</sup> · E. L. Petersen<sup>2</sup>

Received: 29 November 2019 / Revised: 3 July 2020 / Accepted: 11 July 2020 / Published online: 3 August 2020  
© Springer-Verlag GmbH Germany, part of Springer Nature 2020

## Abstract

Experiments on flame propagation and detonation onset behind two solid obstructions were carried out in premixed stoichiometric hydrogen–oxygen mixtures at 20 kPa in a closed-ended tube. Obstacles with three different blockage ratios (25%, 40%, and 80%) were used, and the arrangement between the obstacles was changed in terms of blockage distribution (increasing, decreasing, and equivalent); obstacle distance (38, 76, and 114 mm); and opening geometry. Changes in the obstacle pair characteristics resulted in shocks with distinct intensities and averaged Mach numbers,  $\overline{M}_s$ , that propagated into the undisturbed mixture;  $\overline{M}_s$  varied from 1.3 to 4.5 for the range of obstacle pairs tested. Four distinct deflagration-to-detonation transition (DDT) timescale groups were identified with average values varying between 0.7 and 12 ms. Obstacle pairs with increasing blockage ratio (25–80% and 40–80%) resulted in jet ignition downstream of the second obstacle, reducing the DDT length and timescale significantly when compared to the other obstruction combinations investigated. Soot foil records showed that detonation onset was via ignition from one or more hot spots near the flame front for all obstacle pairs that resulted in jet ignition. The results from this work suggest that channels with irregular obstacle patterns can experience faster detonation onset depending on the position of the obstructions relative to the ignition point.

**Keywords** Flame acceleration · Deflagration-to-detonation transition · Hydrogen · Detonation onset

## 1 Introduction

Detonation initiation and conditions leading to a self-sustained detonation wave are critical for explosion safety applications [1]. A recent review of vapor cloud explosion incidents at industrial sites revealed numerous instances where

detonations occurred with disastrous consequences [2]. For example, the ignition of a large gasoline vapor cloud at an oil terminal in Buncefield, UK, in 2006, created a flame that propagated more than 100 m and eventually detonated, destroying onsite buildings and equipment. Another well-known case is the Fukushima Daiichi nuclear power plant incident in the aftermath of the 2011 tsunami in Japan. The core melt in Unit 1 released hydrogen that accumulated on top of the reactor building and exploded approximately 25 h after station blackout [3]. Strong pressure loads generated from the confined explosion caused severe structural damage to Unit 1 followed by a sequence of explosions inside the other units. These events highlight the importance of mitigating detonations.

Although detonation waves can be generated by different means, deflagration-to-detonation transition (DDT) is the most likely mechanism in industrial explosions [4]. During DDT, a slow flame front is initially generated and accelerates throughout the reactive gas medium due to flame area enhancement and flow interactions with structures and confinement within the flame path. As combustion progresses, the accelerating deflagrative front becomes turbulent,

---

This paper is based on work that was presented at the 25th International Colloquium on the Dynamics of Explosions and Reactive Systems, Beijing, China, July 28–August 2, 2019.

---

Communicated by G. Ciccarelli.

---

**Electronic supplementary material** The online version of this article (<https://doi.org/10.1007/s00193-020-00959-8>) contains supplementary material, which is available to authorized users.

---

✉ E. L. Petersen  
epetersen@tamu.edu

<sup>1</sup> Artie McFerrin Department of Chemical Engineering, Texas A&M University, College Station, TX, USA

<sup>2</sup> J. Mike Walker '66 Department of Mechanical Engineering, Texas A&M University, College Station, TX, USA

creating pressure waves that eventually coalesce, forming a leading shock wave downstream the flame. This leading shock compresses and preheats the reactive gas until a local explosion is initiated via autoignition, and a self-sustained detonation wave is formed [5].

The processes leading to flame acceleration and detonation onset are dependent on the geometry [6]. In obstacle-laden channels, flow disturbances and turbulence generated downstream of the solid obstructions control the overall reaction rate, the size of sensitized mixtures, and shock–flame interactions, which in turn influence terminal flame speeds or under certain conditions flame quenching [7–10]. Comprehensive studies of DDT in cylindrical tubes equipped with repeating orifice plates have demonstrated the impact of obstacle blockage ratio (BR) and spacing between consecutive plates ( $S$ ) on detonation initiation and propagation [11–14]. Peraldi et al. [11] observed the transition of fast flames to detonation propagation when the unobstructed obstacle dimension,  $d$ , exceeded the detonation cell length,  $\lambda$ . The authors then proposed the criterion for DDT in obstructed tubes,  $d/\lambda > 1$ . Subsequent investigations in cylindrical tubes and rectangular channels have shown the high dependency of this critical  $d/\lambda$  parameter on obstruction characteristics [7, 15]. For instance, blockage ratios greater than 60% require significantly larger values for detonation onset, as high as  $d/\lambda = 7$ . For empty channels and tubes equipped with Shchelkin spirals, on the other hand, the minimum DDT criteria were found to be as low as  $1/\pi$  and 0.7, respectively [16]. Recent work combining high-speed schlieren images with soot foil techniques has also revealed that BR influences shock–obstacle interactions, determining whether the local explosion occurs at the obstacle face or near the flame front [17, 18].

In addition to the transverse  $d/\lambda$  criterion, Dorofeev et al. [19] proposed a characteristic size factor  $L$ , considering not only obstacle spacing  $S$ , but also the unobstructed obstacle dimension  $d$  and the channel height  $H$ , to determine the potential for detonation wave formation. According to the authors, this  $L$  dimension represents “the possible macroscopic size of the sensitized mixture in which detonation might originate and develop” and can be defined as follows for obstructed channels:

$$L = \frac{S + H}{2\left(1 - \frac{d}{H}\right)} \quad (1)$$

Their review of large- and small-scale experiments on limiting conditions for DDT suggested that  $L/\lambda > 7$  is a reasonable correlation for detonation preconditioning.

Despite this extensive effort to understand the role of obstructions on DDT, studying DDT in the presence of irregular obstacle patterns has been less explored [20, 21]. To further evaluate irregular obstacle patterns, obstacle

geometry characteristics have been gathered and reviewed for different scales. An obstacle irregularity index, OI, is proposed using the standard deviation of consecutive obstacle characteristic length sizes normalized by  $\lambda$ :

$$OI = \frac{1}{\lambda} \sqrt{\frac{\sum (L_i - \bar{L})^2}{N}} \quad (2)$$

where  $N$  is the number of channel segments or rooms,  $L_i$  is the characteristic length size of the  $i$ th room, and  $\bar{L}$  is the averaged characteristic length size of the experimental setup.

The variation of the irregularity index OI with  $\bar{L}$  for different experiments from the literature is shown in Fig. 1. The vast majority of the cases analyzed presented OI below 0.1 or equal to zero, indicating uniform obstacle arrays. Consequently, limited knowledge of detonation onset under irregular obstruction distributions is available. The circles represent the capabilities of the current experimental setup based on previous studies [21, 22]. Rosas-Martinez [21] utilized the current setup to identify non-uniform obstacle patterns that enhance or weaken flame acceleration. The characteristic length was maintained around 200–400 mm, while OI was greater than 10. Experiments were carried out with three different oxygen–fuel mixtures (hydrogen, acetylene, and ethylene) at stoichiometric concentrations and ignited in the presence of nine metal obstacles distributed within 1 m from the ignition point. Nine distinct obstacle arrays were tested with different obstacle shapes and variable blockage ratio and spacing between consecutive obstructions. The obstacle array with a decreasing BR pattern and a “staggered” obstacle separation showed a tendency to minimize DDT run-up distance; however, due to the limited number

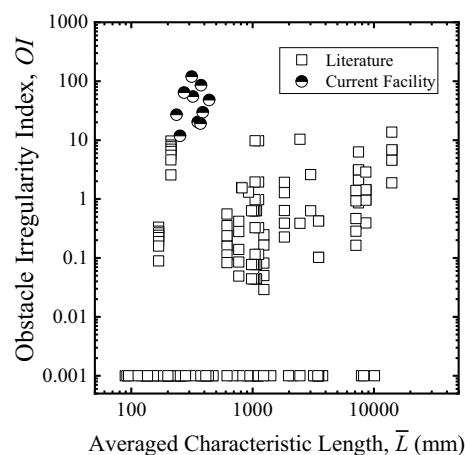


**Fig. 1** Variation of obstacle irregularity index (OI) with averaged characteristic length ( $\bar{L}$ ). For conditions with uniform obstacle pattern (OI = 0), OI was assumed to be 0.001 due to the logarithm scale on the y-axis. A detailed list of references is provided in the supplementary material with OI data labeled

of conditions tested, the authors were unable to identify the dominant factor behind DDT enhancement.

This work is a follow-up to the previous investigation by Rosas-Martinez [21] of detonation onset behind obstacles with irregular obstacle openings and spacing. The number of obstructions was reduced to two in order to identify obstruction characteristics that enhance detonation onset and have a significant impact on the flow field behind the secondary obstruction. First, a summary of the experimental details is provided including the detonation tube layout, test procedures, and new obstacle shapes. The remainder of the paper then presents and discusses in depth the experimental results pertaining to the flame acceleration and the detonation onset as a function of the obstacle configurations.

## 2 Experimental details

Experiments were carried out in a 2.75-m-long horizontal, stainless steel tube with a 38 mm internal diameter and a wall thickness of 1.1 cm (Fig. 2). The tube was closed at both ends, and ignition was via a low-voltage, automotive glow plug operated at 10 A, positioned centrally at the endplate. A modest dump volume was located at the endwall, opposite to the ignition point, to minimize disturbances from shocks reflecting from the endwall; the dimensions of the cylindrical dump tank are specified in Fig. 2. The pressure was recorded at seven different locations along the tube (P1–P7) using piezoelectric pressure transducers (model 113B22, PCB Piezotronics, Inc.) with a measurement range of 34.5 MPa, a rise time smaller than 1  $\mu$ s, and a resonance frequency  $\geq$  500 kHz. Data were recorded using

a PC oscilloscope board (GaGeScope) at a sampling rate of 1 MHz. Considering a one-dimensional coordinate system (in the  $x$ -direction) with an origin at the ignition wall, the locations of the pressure sensors were at  $x=270$ , 525, 780, 1030, 1500, 1960, and 2570 mm. Pressure transducers were the primary diagnostic, and the DAQ system was triggered after a 2% pressure increase at P1 due to compression waves ahead of the flame front.

All tests were conducted at ambient temperature, roughly 20 °C, with stoichiometric hydrogen–oxygen mixtures,  $\phi = 1$  and 20 kPa. The test mixture was prepared by the method of partial pressures in a separate mixing tank and left overnight for complete mixing; tubing positioned at 460 mm, between P1 and P2, was utilized to transfer the test mixture to the detonation tube. The uncertainty of the pressure measurement associated with the mixture tank was  $\pm 0.7$  kPa. The resulting uncertainty of the equivalence ratio due to pressure measurement was  $\pm 0.005$ . For each test, the tube was evacuated to at least 0.03 kPa before being filled with the test mixture up to the target initial pressure.

Two round-edged obstacles with 5 mm thickness and distinct opening shapes were inserted to investigate the impact of varied obstruction characteristics. Three types of obstacle openings were selected with different geometries and degree of flow obstruction (Fig. 3). These shapes differ from symmetrical orifice rings and have been demonstrated to increase run-up distances when compared to regular obstruction arrays [21]. Each obstacle pair was connected by a threaded rod with a 5 mm external diameter. The first obstacle was fixed at 80 mm from the ignition point to allow the formation of a turbulent flame brush prior to the first obstruction [23]. The arrangement between obstructions

**Fig. 2** Schematic of the detonation tube utilized during experiments and the expansion volume located at the endwall

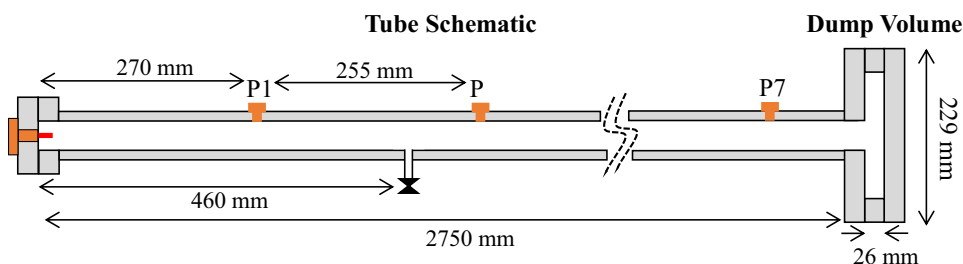
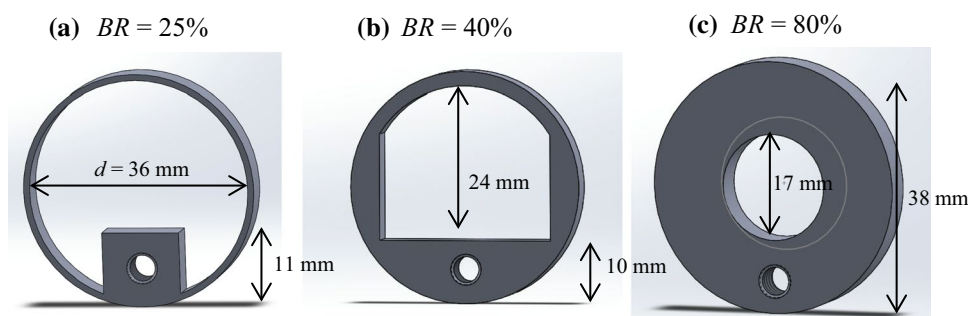


**Fig. 3** Dimensions of the round-edged obstacles inserted inside the detonation tube: **a** obstacle with 25% BR and a solid rectangle, **b** obstruction with 40% BR and square opening, and **c** orifice-type obstacle with 80% BR;  $d$  is the maximum obstacle opening dimension



in the test vessel was changed in terms of blockage ratio (increasing, decreasing, and equivalent), opening geometry, and obstacle separation distance (38, 76, and 114 mm). Table 1 summarizes all conditions tested in this study; a full factorial design was conducted, resulting in 27 different experimental conditions. Each experimental condition was repeated at least three times.

Figure 4 depicts the obstacle pair placement inside the tube during experiments in comparison with the P1 location. Obstacles pairs are named based on the blockage ratio of

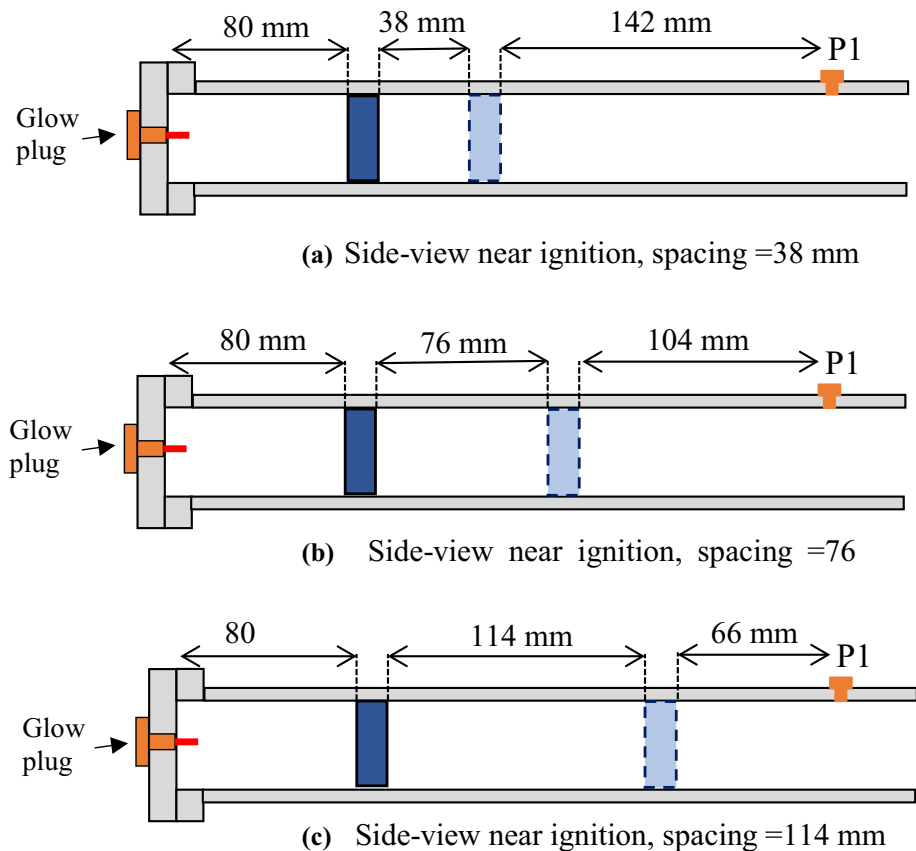
their first and second obstacles, respectively. For instance, the obstacle pair 40–80 represents an obstacle with 40% BR nearest the ignition point followed by one with 80% BR.

Curved aluminum soot foils were inserted in the bottom of the tube, occupying half of the tube circumference to record the detonation structure downstream of the second obstruction. Foils were made from grade 1100 aluminum with 0.5 mm thickness and were inserted according to the expected run-up distance observed from earlier experiments with similar conditions.

**Table 1** Summary of experimental conditions

Test gas	Obstacle spacing, $S$ (mm)	Obstacle pair		
		1st obs. BR	2nd obs. BR	Pair nomenclature
$2\text{H}_2 + \text{O}_2$ , 20 kPa, room temperature	38, 76, and 114	25	25	25–25
			40	25–40
			80	25–80
		40	25	40–25
			40	40–40
			80	40–80
		80	25	80–25
			40	80–40
			80	80–80

**Fig. 4** Representation of obstacle placement for different obstacle spacings: **a**  $S=38$  mm, **b**  $S=76$  mm, and **c**  $S=114$  mm



### 3 Results and discussion

#### 3.1 Flame acceleration without obstacles

Experiments with the smooth tube were initially conducted to assess the DDT run-up distance and DDT time in the absence of obstructions. Pressure records and local average wave speeds along the tube length are shown in Fig. 5. Pressure front velocities were estimated by averaging shock time of arrival between pressure sensors, with the local average value attributed to the second sensor from each pair.

A precursor compression shock traveling toward the dump tank was observed before detonation onset (Fig. 5a). This leading shock initially propagates at speeds above the sonic velocity in the reactants followed by slight deceleration as it approaches the end of the tube. The precursor shock had an average Mach number of around 1.3 and overpressure recordings of about 1.4 of the initial pressure. Similar behavior was reported for experiments with hydrogen–air [24] and hydrogen–oxygen [25] mixtures in smooth tubes. According to the authors, multiple acoustic waves are generated during the early stages of flame acceleration, propagating at higher speeds relative to the reaction front. These waves eventually coalesce, forming a shock. The shock acceleration within the first half of the tube indicates a flame propagating near the pressure front, forming a flame–shock structure. In the second half of the tube, on the other hand, the gap between the pressure front and the flame increases, resulting in a reduction in the shock speed.

Detonation onset occurred far behind the precursor compression wave, after a delay of approximately 25 ms. Soot foil records near the end of the tube showed a regular cellular pattern (Fig. 6), confirming a multi-head detonation structure. The measured average cell width was  $8 \pm 2$  mm, which corroborates experimental measurements

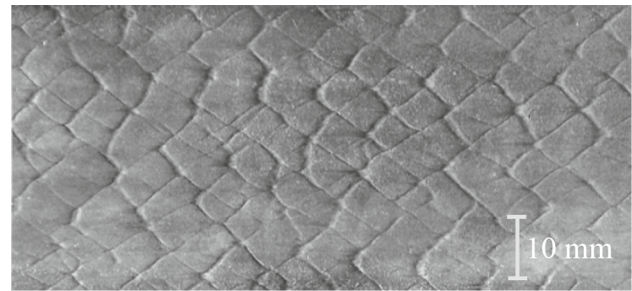


**Fig. 6** Detonation cell size measurements for hydrogen–oxygen mixture at 20 kPa. Test was conducted with the smooth tube; the soot foil was inserted upstream of the expansion section

with similar mixture conditions [26]. DDT was thereby confirmed in the unobstructed tube, which agrees with the detonation onset criteria for smooth channels,  $D \geq \lambda/\pi$  [16].

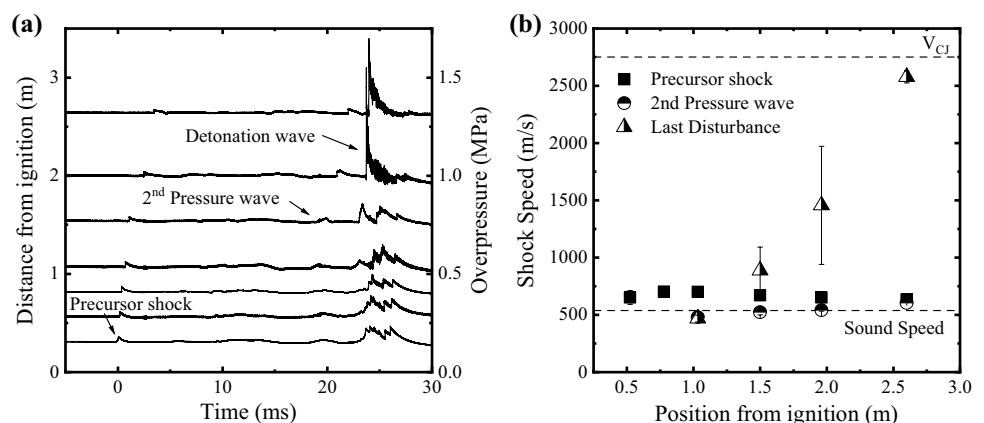
The lack of flame tracking instrumentation along the tube did not allow a precise evaluation of flame position and DDT run-up distance. To overcome this limitation, detonation onset location and timing were estimated by linearly extrapolating the trajectory lines for both detonation and retonation waves (Fig. 7). Using this method, DDT length was estimated to be  $1.7 \pm 0.4$  m from the ignition point for the smooth tube. Additionally, the incident shock time of arrival varied linearly with position. Thus, a global averaged Mach number ( $\overline{M}_s$ ) for the lead shock was assessed based on the inverse of the line slope  $a_1$  ( $10^{-3}$  s/m):

$$\overline{M}_s = \frac{1/a_1}{c} \cdot 10^3 \quad (3)$$

For the smooth tube condition,  $\overline{M}_s$  was  $1.27 \pm 0.01$ .

Since a strong shock wave was created prior to the detonation onset, we believe DDT occurred due to interactions between the boundary layer originating behind the incident shock and the flame front [27]. It was reported by Kuznetsov

**Fig. 5** Results for a stoichiometric hydrogen–oxygen mixture initially at 20 kPa and with the smooth tube: **a** pressure reading along the tube and **b** pressure wave speed estimation





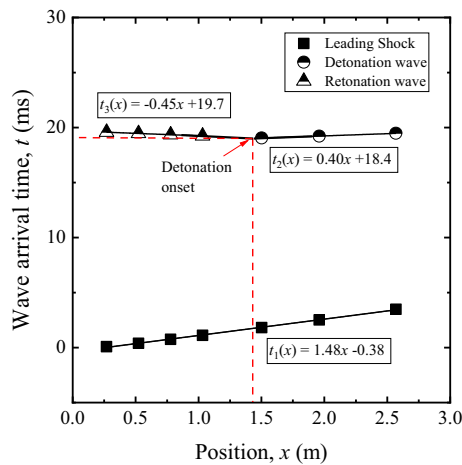


**Fig. 7** Trajectory lines for lead shock, retonation wave, and detonation wave for test with the smooth tube. Linear regression was employed to estimate average speeds, run-up distance, and DDT time

et al. [25] and Ishihara et al. [28] that the structure of the boundary layer influences the time required for detonation onset and run-up distance. As the flame interacts with a turbulent boundary layer, distortions of the flame surface are intensified leading to an abrupt detonation onset. However, if the boundary layer is laminar, flame distortions are negligible, and a longer time is needed for detonation onset. To evaluate the flow regime in the boundary layer behind the incident shock, the Reynolds number,  $Re_0$ , was estimated via [29]:

$$Re_0 = \frac{(V_s - u_2) \left( \frac{\rho_2}{\rho_1} - 1 \right)^2}{\frac{\rho_2}{\rho_1} \nu_2} L \quad (4)$$

where  $V_s$  is the lead shock velocity,  $u_2$  is the gas flow behind the shock,  $\nu$  is the kinematic viscosity,  $\rho$  is the fluid density, and  $L$  is the distance behind a shock wave. Subscripts 1 and 2 represent the states ahead and behind the incident shock wave, respectively. For the sake of simplicity, (4) assumes a stationary flow velocity between the incident shock and the flame front. It is worth noting that, during flame acceleration, flame speeds are not constant and increase with time. However, the difference between the lead shock and flame speeds is relatively close to the flow velocity, which makes (4) valid for conservative estimates [25]. In the present work,  $Re_0 \geq 2.5 \times 10^6$  for  $L \geq 0.8$  m. Experimental data reported by [30] show that the transition Reynolds number,  $Re_t$ , is approximately  $0.5 \times 10^6$  for  $M_s \approx 1$ . Consequently, it is reasonable to assume that the boundary layer is fully turbulent at distances of approximately 0.8 m behind the incident shock given that  $Re_0 > 5Re_t$  [29].

According to Kuznetsov et al. [25], the size of the boundary-layer thickness dictates the scale of turbulent pulsations,

which in turn impacts detonation onset characteristics. The turbulent boundary-layer thickness,  $\delta_t$ , can be determined from the classical theory of the turbulent boundary layer by applying expressions for  $\delta_t$  with logarithm accuracy (see [25, 31] for more details). The following equation was derived by rearranging the simplified model proposed by Kuznetsov et al. [25] assuming a constant shock speed flow along a wall with roughness  $\epsilon$ :

$$\frac{C \cdot L}{\delta_t} - \frac{1}{k} \ln \left( \frac{\delta_t}{\epsilon} \right) - K = 0 \quad (5)$$

where  $C$ ,  $k$ , and  $K$  are empirical parameters,  $L$  is the distance between the incident shock and reaction front, and  $\epsilon$  is the tube roughness. Note that the application of (5) is conservative and assumes that the flame front is located midway between ignition position and lead shock [24].

Equation (5) can be solved implicitly to estimate the distance,  $x_{\max}$ , at which point the turbulent boundary layer thickness reaches its maximum value,  $\delta_t = D/2$ . Beyond  $x_{\max}$ ,  $\delta_t$  assumes the same order of magnitude as the internal tube diameter, and DDT is facilitated due to flame interaction with the boundary layer. Taking the empirical parameters to be  $K = 5.5$ ,  $k = 0.4$ , and  $C = 0.3\sqrt{2}$  (as suggested by Landau and Lifshitz [31]) and using a typical roughness for stainless steel of  $\epsilon = 0.05$  mm,  $x_{\max}$  was estimated to be 0.9 m. Therefore,  $\delta_t$  is maximized when a distance of 0.9 m between the lead shock and the flame front is reached for the experimental conditions; this requires that the flame propagates at least 0.9 m prior to detonation onset, which agrees with experimental observations for the run-up distance in the smooth tube. This result supports the argument that detonation occurred in a region of relatively high turbulence levels inside the tube.

Due to the short tube length and large delay time, reflections from the expansion volume might also have contributed to local explosions via shock focusing. Small perturbations can be noticed propagating from the dump tank to the ignition point during the time interval before detonation onset. As stated by Salamandra et al. [32], detonation onset is facilitated in short tubes because of the interaction between reaction front and reflected compression waves.

## 3.2 Detonation onset behind two obstacles

### 3.2.1 Effect of obstacle-induced shock speed on DDT time and run-up distance

DDT was observed in all cases with an obstacle pair inserted in the combustion chamber; however, the detonation initiation time and run-up distance varied significantly according to the strength of the shock created behind the second obstruction. The estimated detonation onset time

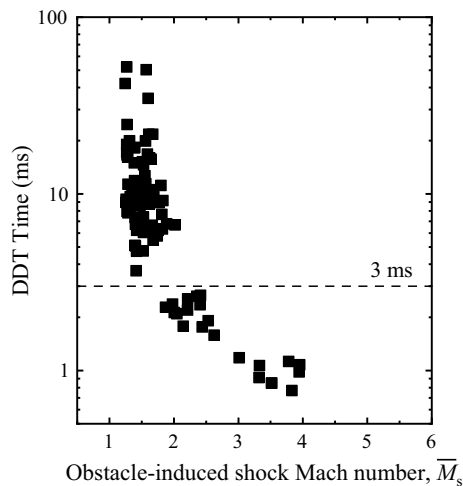


**Fig. 8** Variation of DDT time with pre-DDT average shock Mach number

versus the averaged Mach number of the shock,  $\overline{M}_s$ , for different obstacle pairs is provided in Fig. 8. In this section,  $\overline{M}_s$  is calculated for the shock formed downstream of the second obstruction prior to DDT and varied from 1.3 to 4.5 for the range of obstacle pairs tested.

The obstruction pairs 25–80 and 40–80 separated at 76 and 114 mm experienced detonation initiation before the first or second pressure sensors (P1 or P2). For those conditions, the lack of signs for a retonation wave or a compression front made it difficult to estimate precisely both  $\overline{M}_s$  and DDT time based on the methodology applied; for the run-up distance quantification, soot foil measures were employed.

A reduction in DDT time with increasing  $\overline{M}_s$  is seen in Fig. 8. A clear distinction can be made between detonation onset time above and below 3 ms. This disparity is attributed to flame interactions, even if minimal, with reflected shocks from the dump tank for pressure fronts with relatively low Mach numbers. Incident shocks with  $\overline{M}_s$  below 2 required approximately 3 ms to reach the tube end; consequently, tests with detonation initiation time exceeding 3 ms exhibit significant variability. Numerical simulations have shown that multiple shock–flame interactions in the turbulent flame brush create fluctuations in temperature, density, and pressure that propagate throughout the system [33]. As these fluctuations are intensified in the remaining unburned mixture, regions of accelerated reaction rates are created (hot spots). The mechanism of hot spot generation from flame interaction with reflecting waves is extremely stochastic and difficult to control. The final hot spot location depends on the flame position, shock intensity, and number of interactions between reflecting waves and the incident flame front. These factors may change even for

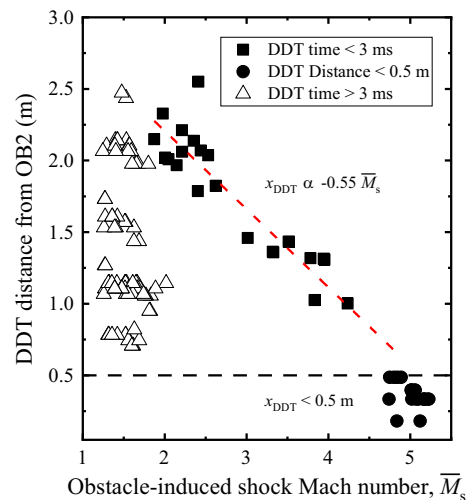


**Fig. 9** Variation of DDT distance with pre-DDT average shock Mach number

tests with similar initial conditions, producing significant scatter in the DDT time data for weak shocks downstream of the obstacle pair,  $\overline{M}_s < 2$ .

The dependence of run-up distance with the lead shock Mach number,  $\overline{M}_s$ , is plotted in Fig. 9. Some variability in the data is observed for tests with DDT time greater than 3 ms due to flame interaction with reflecting pressure waves, as explained previously. Nonetheless, the data correlate fairly well in the region with a relatively high Mach number,  $\overline{M}_s > 2$ . Data points at which detonation onset happened before P2 ( $x_{DDT} < 0.5 \text{ m}$ ) were excluded due to the lack of precision on the incident Mach number. The dependence of the run-up distance downstream of the second obstruction,  $x_{DDT}$ , on lead shock Mach number was found to be close to linear:  $x_{DDT}(\text{m}) = (3.3 \pm 0.1) - (0.55 \pm 0.04)\overline{M}_s$ , where uncertainties were defined by the standard regression analysis.

### 3.2.2 Impact of obstacle pair on $P_{\max}$ at P1

In an attempt to understand the influence of each obstacle pair on incident wave intensity, the change in maximum pressure at P1 ( $P_{1,\max}$ ) was investigated. The variation of  $P_{1,\max}$  with the averaged blockage ratio across the obstacle pair for tests with  $S = 76 \text{ mm}$  is shown in Fig. 10. This distance is equivalent to two internal diameters, and the average BR is simply the arithmetic mean between the blockage ratio of the two obstructions. For instance, the obstacle pair 40–80 would have an average BR of 60%, similar to the 80–40 pair.

The observed trend is comparable to tubes filled with constant geometry obstacles [7]. First,  $P_{1,\max}$  rises as averaged BR varies from 0 to 60% due to higher turbulence intensities which enhance mixing between reactants and accelerates

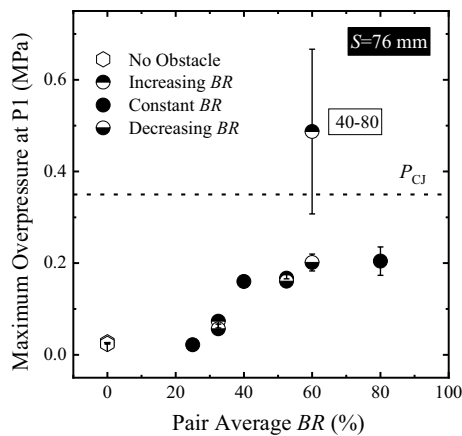


**Fig. 10** Variation of maximum overpressure with average BR at first pressure sensor ( $P_{1,max}$ ) located 270 mm from the ignition point and 104 mm downstream of the second obstacle. Spacing between obstacles was maintained as 76 mm, while blockage ratio and obstacle shape were varied

reaction rate. Then, as average BR further increases from 60 to 80%,  $P_{1,max}$  reduces likely due to flame deceleration as a result of momentum losses and larger unreacted pockets behind the obstruction with high BR. One can also observe that obstacle pairs 40–25 and 25–40 presented a negligible variation on  $P_{1,max}$ , indicating no significant changes in the turbulence levels within 104 mm from the second obstacle. Conversely, obstacle 40–80 with a sharp increase in BR across the pair resulted in overpressures above the Chapman–Jouguet detonation pressure, indicating detonation initiation near P1. Detonation initiation for 25–80 happened between P1 and P2 but relatively near the second obstruction.

This detonation onset shortly after an obstruction with high BR is analogous to jet initiation in confined geometries [34]. In this case, a turbulent jet of combustion products is generated as the flame front passes the last obstacle. The jet experiences lateral expansion, and it is preceded by a strong obstacle-induced compression wave. As this shock reflects from the confinement walls, localized explosions are induced due to the interactions between the turbulent flame front and the reflected waves [18]. Dorofeev et al. [35] proposed a minimum jet initiation criterion for unconfined jets based on obstacle opening  $d$  and cell size,  $d/\lambda > 7$ . In tubes with small internal diameter, the cooling effects from jet expansion are reduced, and stronger interactions between the turbulent jet and reflected waves are observed. Therefore, the criterion for jet ignition is expected to be below 7 for tubes with small dimensions. For the pair experiencing jet ignition (40–80 and  $S=76$  mm), the obstacle opening and distance between the second obstruction and P1 were about 2.2 times and 13 times greater than the cell width, respectively. Even though  $d_2/\lambda$  was below the criterion proposed

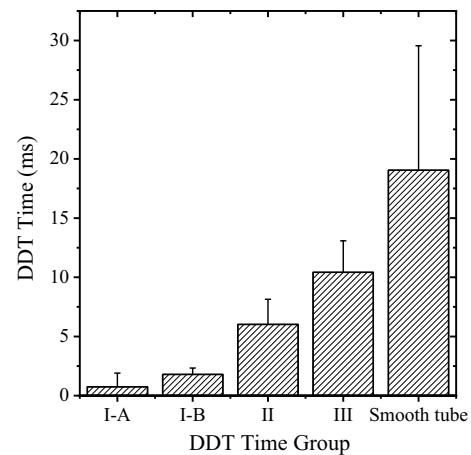


**Fig. 11** Variation of average DDT timescale for each group identified. Results for the smooth tube conditions are included as a reference

by Dorofeev et al. [35], sufficient length was available for detonation initiation.

### 3.2.3 DDT timescales and pressure profiles

Overall, four distinct DDT timescale groups were identified with average values varying between 0.7 and 12 ms (Fig. 11). Case I-A had the fastest detonation initiation observed. Plots of pressure profile along the tube length and wave speeds for case I-A are shown in Fig. 12. In this condition, a strong shock is created in the wake of the second obstacle and propagates at almost constant velocity, near the CJ detonation value. Since detonation onset occurred before P1 or P2, no clear sign of a retonation wave traveling backward toward the ignition point was identified (Fig. 12a). DDT onset time was then related to the time of maximum pressure intensity in P1.

Readings from wall-mounted soot foils behind the second obstacle for obstacle pairs that resulted in case I-A are provided in Figs. 13 and 14. Detonation onset was demonstrated to be qualitatively similar for both instances, via the ignition of one or multiple hot spots near the tube wall downstream of the second obstruction (OB2). For pair 40–80 and  $S=76$  mm (Fig. 13), detonation is initiated from a local explosion created in the centerline of the tube in the proximity of the reaction front. Multiple fine white streaks oriented in the flow direction are observed approximately 100 mm behind OB2 and can be traced to the flame front position prior to detonation onset [36]. As the local explosion wave propagates transversely, it collides with the tube wall forming a subsequent hot spot. Since there is no sign of lateral shock collision, a possible explanation for the hot spot generation is via shock reflection with the tube wall [37]. For pair 25–80 and  $S=76$  mm (Fig. 14), two hot spots were created via shock focusing of transverse waves reflecting



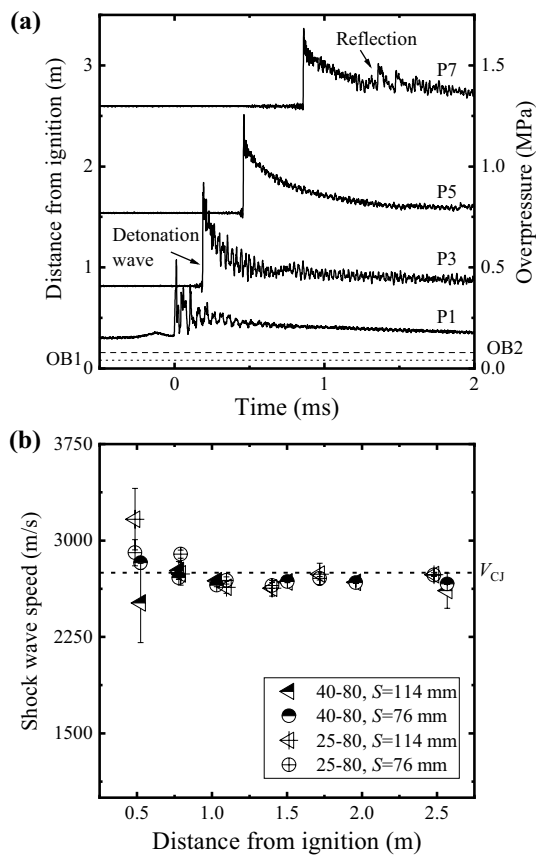


**Fig. 12** Results for obstacle pairs that resulted in detonation onset prior to P1: **a** pressure reading for pair 40–80 and  $S=114$  mm, and **b** estimated shock wave speed along the tube

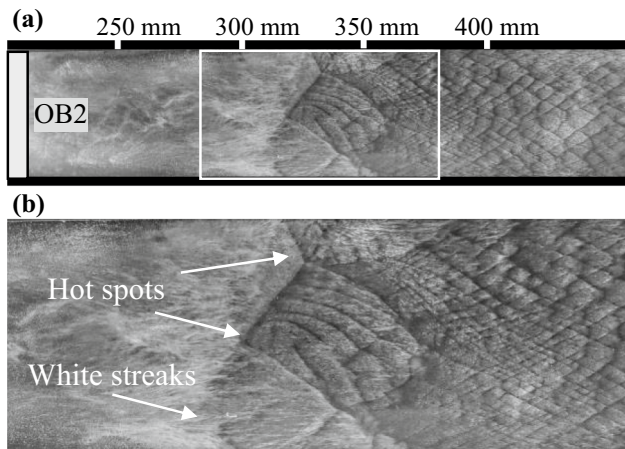


**Fig. 13** Soot track for pair 40–80 and  $S=76$  mm. The soot foil was inserted behind the second obstruction on the tube bottom. Distance measurements are relative to the ignition point

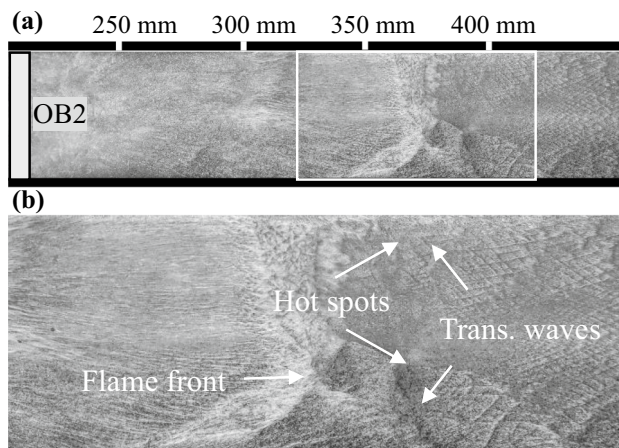


**Fig. 14** Soot track for pair 25–80 and  $S=76$  mm. The soot foil was inserted behind the second obstruction on the tube bottom. Distance measurements are relative to the ignition point

from both sides of the confinement walls and a pressure front ahead of the flame brush. Small, cellular patterns can be seen emanating from the two shock focusing points, indicating an overdriven detonation.

In case I-B, a strong obstacle-induced pressure wave is evident propagating above the sonic speed toward the end-plate; a local explosion occurs somewhere after P2, generating a detonation wave that overtakes the leading shock (Fig. 15). Soot foil measurements in Fig. 16 indicate detonation initiation due to interaction between two oblique transverse shock waves. A DDT line is formed resulting from multiple triple-point trajectories subsequent to the shock collision. Those transverse waves originated via reflection of the lead shock with the confinement wall.

Cases II and III are related to delayed detonations after the lead shock has reached the tube end. Therefore, in both conditions, the hot spot generation was impacted by reflected waves propagating from the expansion section. In case II (see Fig. 17), the obstacle-induced shock presented an initial speed of 1500 m/s near the region behind the obstacle pair followed by a significant deceleration as it continues moving toward the closed end. The intensity of the precursor wave is not sufficient to ignite the mixture via shock compression, and, consequently, detonation initiation occurs at some distance behind the shock front. The substantial decay of the lead shock speed indicates a large gap between the shock and flame front, analogous to the smooth tube condition.

Finally, for condition III, two major pressure waves are observed before the transition to detonation (Fig. 18). Similar to the previous case, the obstacle-induced shock presented an initial high velocity followed by a significant deceleration as a result of the decoupling between flame front and shock front. Subsequently, a second pressure front is created experiencing a minor velocity increase up to 2 m.

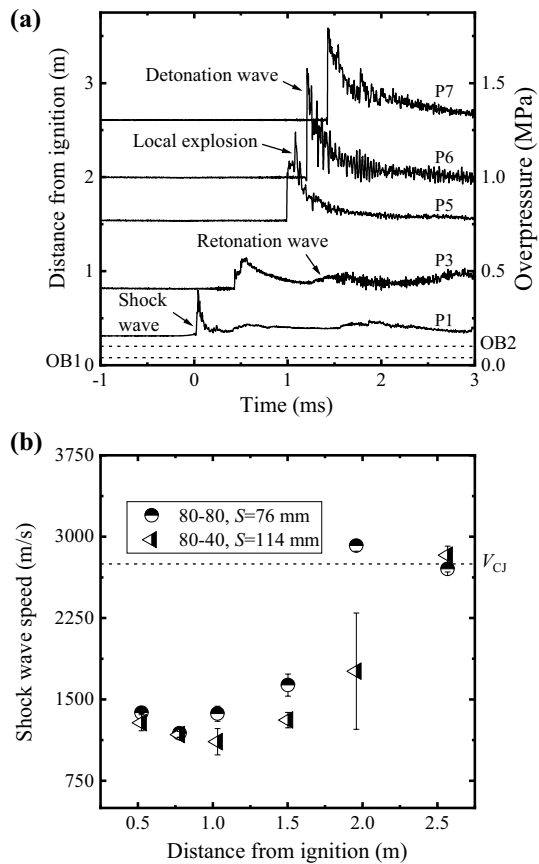


**Fig. 15** a Pressure recordings for pair 80–80 and  $S=76$  mm, and b shock wave speeds along the tube for tests that resulted in case I-B

Both pressure fronts did not trigger local explosions, and detonation onset takes place in the second half of the tube after a delay time of approximately 20 ms. Soot foil readings for pair 80–80 and  $S=38$  mm (Fig. 19) show one hot spot being formed due to shock focusing of two transversal waves. The origin of both waves is not clear since there is no demarcation of flame front as opposed to cases I-A and I-B. The absence of sharp demarcations of the reaction front during hot spot generation indicates that local ignition probably occurred behind the flame.

### 3.2.4 Summary of results

Table 2 summarizes the predominant propagation behavior for each condition tested. Obstructions with a sharp increase in blockage ratio across the obstacle pair (25–80 and 40–80) presented the smallest detonation onset time and distance when compared to the other obstruction pairs investigated. Detonation initiation for both conditions was analogous to jet ignition behind the second obstacle due to the formation of a high-intensity obstacle-induced shock. As the flame front passes a narrower obstruction opening, it generates

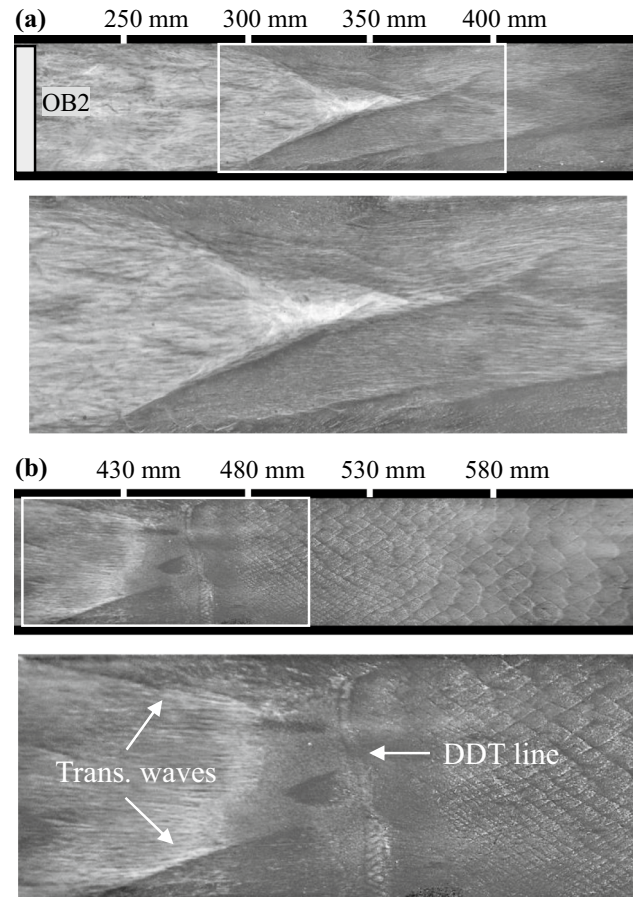


**Fig. 16** Soot track for pair 80–40 and  $S=114$  mm, case I-B. The soot foil was inserted behind the second obstruction on the tube bottom. Distance measurements are relative to the ignition point

strong pressure waves that reflect from the confinement walls and interact with the turbulent flame front. This interaction between the turbulent jet and reflected waves creates local explosions. Another important aspect is the distance between the obstacle and the ignition point—longer spacing results in faster flames before reaching the obstacle surface. For instance, cases with higher BR closer to ignition (80–40 and 80–25) resulted mostly in combustion type III, in which the leading shock front was significantly slower.

It can also be noted that obstacle pairs with the same average blockage ratio resulted in distinct combustion characteristics, especially when BR variation was more abrupt. For instance, comparing the results from the obstacle pair 40–80 with its equivalent on average blockage (but transposed), 80–40, one may observe that the increasing obstruction leads to a stable detonation within the first three sensors. Conversely, in the decreasing blockage case, DDT takes place mostly within the second half of the tube (after P4), and it is preceded by two major pressure waves. Similar conclusions were obtained for obstacle pairs 80–25 and 25–80. Obstacle pairs

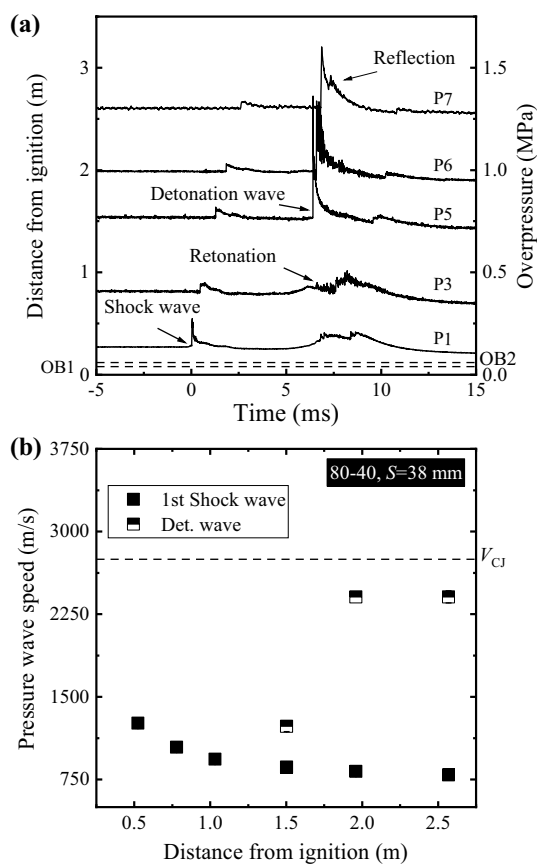


**Fig. 17** Results for pair 80–40 and  $S=38$  mm, case II: **a** pressure recordings, and **b** shock wave speeds along the tube

with smoother changes in BR (40–25 and 25–40) but having the same average BR in general did not demonstrate significant differences in behavior.

In addition to the effects of blockage ratio variation across the obstacle pair, the opening geometry may also have impacted the DDT process. Each obstacle employed has a unique orifice shape that creates different shock structures immediately after the second obstacle. For example, the 80% BR obstacle produces an axisymmetric shock, which differs from the other two. Since shock reflection becomes significant for jet ignition in confined spaces, deviations in shock structure may change shock reflection patterns and, therefore, impact detonation initiation. Further investigation is necessary to study the isolated effect of blockage ratio variation and orifice shape on DDT.

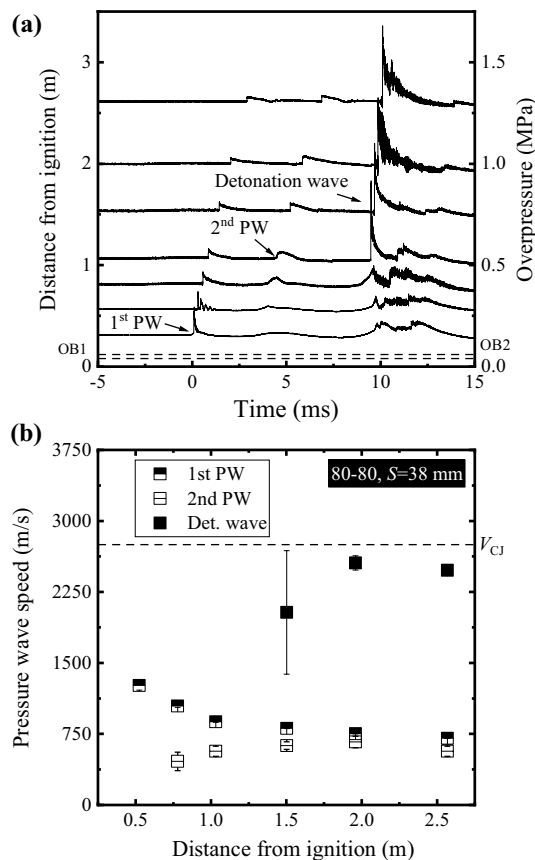


**Fig. 18** Results for pair 80–80 and  $S=38$  mm, case III: **a** pressure recordings and **b** shock wave speeds along the tube. PW stands for pressure wave

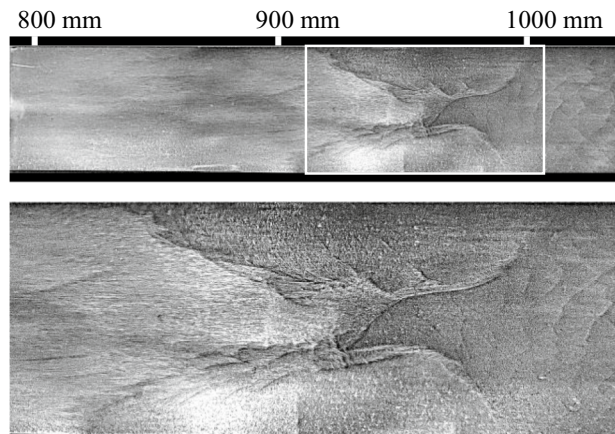


**Fig. 19** Soot track for pair 80–80 and  $S=38$  mm, case III. The soot foil was inserted behind the second obstruction at 800 mm from the ignition point



**Table 2** Summary of prevailing pressure profile for each obstacle pair tested

Obstacle pair	Average BR (%)	$d_2/\lambda$	Obstacle spacing (mm)		
			38	76	114
80–80	80	2.2	II/III	I–B/II	I–B/II
80–40	60	3.2	III	III	I–B/II
40–80	60	2.2	III	I–A	I–A
80–25	53	4.6	III	III	III
25–80	53	2.2	III	I–A	I–A
40–40	40	3.2	III	II	II
40–25	33	4.6	III	III	II
25–40	33	3.2	II	III	III
25–25	25	4.6	III	II	III

## 4 Conclusions

Experiments on flame propagation and DDT were carried out in premixed stoichiometric hydrogen–oxygen mixtures at 20 kPa in a closed tube with two obstacles of varied configuration.

Changes in the obstacle pair characteristics resulted in obstacle-induced shocks with distinct intensities and averaged Mach numbers,  $\overline{M}_s$ , that propagated into the undisturbed mixture;  $\overline{M}_s$  varied from 1.3 to 4.5 for the range of obstacle pairs tested. This work demonstrated that, under the right variation of obstacle characteristics, DDT can be accomplished even with two obstacles near the ignition source for highly reactive mixtures.

Results from the smooth tube condition agreed with the theory of DDT in the turbulent boundary layer. Detonation initiation occurred in the location of maximum turbulent fluctuations where the turbulent layer thickness assumed dimensions equivalent to half of the internal tube diameter.

For tests with obstacle pairs inserted, four distinct DDT timescales were identified based on the average detonation initiation time with values ranging from 0.7 to 12 ms. Additionally, the order of obstacles impacted detonation onset for pairs with one obstacle having a high degree of flow obstruction. Obstacles with a sharp increase in blockage ratio across the obstacle pair (25–80 and 40–80) resulted in detonation onset comparable to the jet ignition case. Conversely, pairs with 80% BR on the ignition source side (80–40 and 80–25) presented weaker incident shocks and, consequently, longer run-up distances.

The results from this work suggest that channels with irregular obstacle patterns can experience faster detonation onset depending on the position of the obstructions relative to the ignition point.

## References

- Dorofeev, S.B.: Flame acceleration and explosion safety applications. *Proc. Combust. Inst.* **33**(2), 2161–2175 (2011). <https://doi.org/10.1016/j.proci.2010.09.008>
- Chamberlain, G., Oran, E., Pekalski, A.: Detonations in industrial vapour cloud explosions. *J. Loss. Prev. Proc. Ind.* **62**, 103918 (2019). <https://doi.org/10.1016/j.jlp.2019.103918>
- TEPCO: Fukushima Nuclear Accident Analysis Report (2012). [https://www.tepco.co.jp/en/press/corp-com/release/betu12\\_e/images/120620e0104.pdf](https://www.tepco.co.jp/en/press/corp-com/release/betu12_e/images/120620e0104.pdf)
- Oran, E.S., Chamberlain, G., Pekalski, A.: Mechanisms and occurrence of detonations in vapor cloud explosions. *Prog. Energy Combust. Sci.* **77**, 100804 (2020). <https://doi.org/10.1016/j.pecs.2019.100804>
- Lee, J.H.: Initiation of gaseous detonation. *Annu. Rev. Phys. Chem.* **28**(1), 75–104 (1977)
- Ciccarelli, G., Dorofeev, S.: Flame acceleration and transition to detonation in ducts. *Prog. Energy Combust. Sci.* **34**(4), 499–550 (2008). <https://doi.org/10.1016/j.pecs.2007.11.002>
- Kuznetsov, M., Alekseev, V., Bezmelnitsyn, A., Breitung, W., Dorofeev, S., Matsukov, I., Vesper, A., Yankin, Y.: Effect of obstacle geometry on behaviour of turbulent flames. RRC “Kurchatov Institute”, Preprint IAE-6137/13 (1999)
- Yu, L.X., Sun, W.C., Wu, C.K.: Flame acceleration and overpressure development in a semiopen tube with repeated obstacles. *Proc. Combust. Inst.* **29**(1), 321–327 (2002). [https://doi.org/10.1016/S1540-7489\(02\)80043-8](https://doi.org/10.1016/S1540-7489(02)80043-8)
- Chao, J., Lee, J.: The propagation mechanism of high speed turbulent deflagrations. *Shock Waves* **12**(4), 277–289 (2003). <https://doi.org/10.1007/s00193-002-0161-2>
- Lee, J.H., Knystautas, R., Chan, C.K.: Turbulent flame propagation in obstacle-filled tubes. *Symposium (International) on Combustion*, vol. 20(1), pp. 1663–1672 (1985). [https://doi.org/10.1016/S0082-0784\(85\)80662-7](https://doi.org/10.1016/S0082-0784(85)80662-7)
- Peraldi, O., Knystautas, R., Lee, J.H.: Criteria for transition to detonation in tubes. *Symposium (International) on Combustion*, vol. 21(1), pp. 1629–1637 (1988). [https://doi.org/10.1016/S0082-0784\(88\)80396-5](https://doi.org/10.1016/S0082-0784(88)80396-5)
- Guirao, C., Knystautas, R., Lee, J.: A summary of hydrogen–air detonations for reactor safety. Sandia National Laboratories/McGill University, Report NUREG/CR-4961 (1989)
- Ciccarelli, G., Wang, Z., Lu, J., Cross, M.: Effect of orifice plate spacing on detonation propagation. *J. Loss. Prev. Proc. Ind.* **49**, 739–744 (2017). <https://doi.org/10.1016/j.jlp.2017.03.014>
- Gu, L.S., Knystautas, R., Lee, J.H.S.: Influence of obstacle spacing on the propagation of quasi-detonation. In: Borisov, A., Kuhl, L., Bowen, J.R., Leyer, J.-C. (eds.) *Dynamics of Explosions*, AIAA, pp. 232–247 (1988). <https://doi.org/10.2514/5.9781600865886.0232.0247>
- Lee, J.H.S., Knystautas, R., Freiman, A.: High speed turbulent deflagrations and transition to detonation in H<sub>2</sub> air mixtures. *Combust. Flame* **56**(2), 227–239 (1984). [https://doi.org/10.1016/0010-2180\(84\)90039-7](https://doi.org/10.1016/0010-2180(84)90039-7)
- Lindstedt, R.P., Michels, H.J.: Deflagration to detonation transitions and strong deflagrations in alkane and alkene air mixtures. *Combust. Flame* **76**(2), 169–181 (1989). [https://doi.org/10.1016/0010-2180\(89\)90065-5](https://doi.org/10.1016/0010-2180(89)90065-5)
- Maeda, S., Minami, S., Okamoto, D., Obara, T.: Visualization of deflagration-to-detonation transitions in a channel with repeated obstacles using a hydrogen–oxygen mixture. *Shock Waves* **26**(5), 573–586 (2016). <https://doi.org/10.1007/s00193-016-0660-1>
- Obara, T., Kobayashi, T., Ohayagi, S.: Mechanism of deflagration-to-detonation transitions above repeated obstacles. *Shock*

- Waves **22**(6), 627–639 (2012). <https://doi.org/10.1007/s00193-012-0408-5>
19. Dorofeev, S.B., Sidorov, V.P., Kuznetsov, M.S., Matsukov, I.D., Alekseev, V.I.: Effect of scale on the onset of detonations. *Shock Waves* **10**(2), 137–149 (2000). <https://doi.org/10.1007/s001930050187>
  20. Frolov, S.M.: Fast deflagration-to-detonation transition. *Russ. J. Phys. Chem. B* **2**(3), 442–455 (2008). <https://doi.org/10.1134/S1990793108030184>
  21. Rosas-Martinez, C.A.: Deflagration-to-detonation transition (DDT) studies: Effect of non-uniform obstacle distribution on DDT. PhD Thesis, Texas A&M University (2016)
  22. Polley, N.L., Egbert, M.Q., Petersen, E.L.: Methods of re-initiation and critical conditions for a planar detonation transforming to a cylindrical detonation within a confined volume. *Combust. Flame* **160**(1), 212–221 (2013). <https://doi.org/10.1016/j.combustflame.2012.09.017>
  23. Clanet, C., Searby, G.: On the “tulip flame” phenomenon. *Combust. Flame* **105**(1–2), 225–238 (1996). [https://doi.org/10.1016/0010-2180\(95\)00195-6](https://doi.org/10.1016/0010-2180(95)00195-6)
  24. Thomas, G., Oakley, G., Bambrey, R.: An experimental study of flame acceleration and deflagration to detonation transition in representative process piping. *Process Saf. Environ. Prot.* **88**(2), 75–90 (2010). <https://doi.org/10.1016/j.psep.2009.11.008>
  25. Kuznetsov, M., Alekseev, V., Matsukov, I., Dorofeev, S.: DDT in a smooth tube filled with a hydrogen–oxygen mixture. *Shock Waves* **14**(3), 205–215 (2005). <https://doi.org/10.1007/s00193-005-0265-6>
  26. Knystautas, R., Lee, J.H., Guirao, C.M.: The critical tube diameter for detonation failure in hydrocarbon–air mixtures. *Combust. Flame* **48**, 63–83 (1982). [https://doi.org/10.1016/0010-2180\(82\)90116-X](https://doi.org/10.1016/0010-2180(82)90116-X)
  27. Nettleton, M.A.: *Gaseous Detonations: Their Nature, Effects and Control*. Springer, Berlin (2012)
  28. Ishihara, S., Tamura, S., Ishii, K., Kataoka, H.: Effects of boundary layer on flame propagation generated by forced ignition behind an incident shock wave. *Shock Waves* **26**(5), 599–609 (2016). <https://doi.org/10.1007/s00193-016-0684-6>
  29. Mirels, H., Mullen, J.F.: Small perturbation theory for shock-tube attenuation and nonuniformity. *Phys. Fluids* **7**(8), 1208–1218 (1964). <https://doi.org/10.1063/1.1711363>
  30. Hartunian, R.A., Russo, A.L., Marrone, P.V.: Boundary-layer transition and heat transfer in shock tubes. *J. Aerosp. Sci.* **27**(8), 587–594 (1960). <https://doi.org/10.2514/8.8656>
  31. Landau, L.D., Lifshitz, E.M.: *Fluid Mechanics*. Pergamon, Oxford (1987). <https://doi.org/10.1016/C2013-0-03799-1>
  32. Salamandra, G.D., Bazhenova, T.V., Zaicev, S.G., Soloukhin, R.I., Naboko, I.M., Sevastyanova, I.K.: *Some Methods for Investigation of Fast-Running Processes*. Acad. Nauk SSSR, Moscow (1960) (in Russian)
  33. Oran, E.S., Khokhlov, A.M.: Deflagrations, hot spots, and the transition to detonation. *Philos. Trans. R. Soc. Lond.* **357**(1764), 3539–3551 (1999). <https://doi.org/10.1098/rsta.1999.0508>
  34. Medvedev, S., Khomik, S., Olivier, H., Polenov, A., Bartenev, A., Gelfand, B.: Hydrogen detonation and fast deflagration triggered by a turbulent jet of combustion products. *Shock Waves* **14**(3), 193–203 (2005). <https://doi.org/10.1007/s00193-005-0264-7>
  35. Dorofeev, S.B., Bezmelnitsin, A.V., Sidorov, V.P., Yankin, J.G., Matsukov, I.D.: Turbulent jet initiation of detonation in hydrogen–air mixtures. *Shock Waves* **6**(2), 73–78 (1996). <https://doi.org/10.1007/BF02515190>
  36. Kellenberger, M., Ciccirelli, G.: Advancements on the propagation mechanism of a detonation wave in an obstructed channel. *Combust. Flame* **191**, 195–209 (2018). <https://doi.org/10.1016/j.combustflame.2017.12.023>
  37. Ciccirelli, G., Cross, M.: On the propagation mechanism of a detonation wave in a round tube with orifice plates. *Shock Waves* **26**(5), 587–597 (2016). <https://doi.org/10.1007/s00193-016-0676-6>

**Publisher's Note** Springer Nature remains neutral with regard to jurisdictional claims in published maps and institutional affiliations.